Method for Characterizing Nanoscale Wear of Atomic Force Microscope Tips

Jingjing Liu,[§] Jacob K. Notbohm,[†] Robert W. Carpick,[‡] and Kevin T. Turner[§,†,*]

[§]Materials Science Program, University of Wisconsin, Madison, Wisconsin 53706, [†]Department of Mechanical Engineering, University of Wisconsin, Madison, Wisconsin 53706, and [‡]Department of Mechanical Engineering and Applied Mechanics, University of Pennsylvania, Philadelphia, Pennsylvania 19104

ARTICLE

ABSTRACT Atomic force microscopy (AFM) is a powerful tool for studying tribology (adhesion, friction, and lubrication) at the nanoscale and is emerging as a critical tool for nanomanufacturing. However, nanoscale wear is a key limitation of conventional AFM probes that are made of silicon and silicon nitride (SiN_x). Here we present a method for systematically quantifying tip wear, which consists of sequential contact-mode AFM scans on ultrananocrystalline diamond surfaces with intermittent measurements of the tip properties using blind reconstruction, adhesion force measurements, and transmission electron microscopy (TEM). We demonstrate direct measurement of volume loss over the wear test and agreement between blind reconstruction and TEM imaging. The geometries of various types of tips were monitored over a scanning distance of approximately 100 mm. The results show multiple failure mechanisms for different materials, including nanoscale fracture of a monolithic Si tip upon initial engagement with the surface, film failure of a SiN_x-coated Si tip, and gradual, progressive wear of monolithic SiN_x tips consistent with atom-by-atom attrition. Overall, the method provides a quantitative and systematic process for examining tip degradation and nanoscale wear, and the experimental results illustrate the multiple mechanisms that may lead to tip failure.

KEYWORDS: tip · wear · atomic force microscopy · nanotribology · probe

Atomic force microscopy (AFM) is a powerful tool for high-resolution characterization of surfaces, nanotribology investigations, and nanoscale manufacturing. The resolution of AFM-based measurements is critically dependent on the geometry of the probe tip and is strongly affected by the degradation of the tip through processes such as wear. The durability of the tip and an understanding of the processes that lead to changes in tip geometry have taken on greater importance recently as nanoscale tips are increasingly being used in metrology, manufacturing, and device applications in which a single probe may be used numerous times and scanned over distances of millimeters to kilometers during its life. Specific applications that push the limits of tip durability include nanolithography,[1−3] tip-based nanomanufacturing,[4] nanoscale metrology for the semiconductor industry,[5,6] and probe-based data storage.[7,8]

There is a critical need for experimental methods that allow for the systematic evaluation of the life span of nanoscale tips and permit the assessment of new types of probes made of more wear-resistant materials, such as carbon-based materials.[9,10] In the present work, we report a quantitative experimental approach for characterizing the wear of atomic force microscope probes. Using a combination of techniques, the evolution of the geometry and surface properties of the tip are quantified as a function of scanning distance. The method is demonstrated by measuring wear of conventional silicon and silicon nitride tips.

There are several reports in which the wear of atomic force microscope tips has been investigated. Early studies examined the wear of silicon nitride (SiN_x) tips scanned on silicon (Si) surfaces under applied loads of 20−100 nN.[11,12] Changes in tip geometry were characterized by direct imaging with another AFM tip[11] and by inverse imaging using an etched Si surface for tip characterization.[12] The observed changes in tip geometry were attributed to several wear mechanisms, including adhesion, plastic deformation, and low cycle fatigue.[11,12] More recent work has explored wear under different environmental conditions, including different temperatures, humidity, background gases (laboratory air, dry nitrogen), and liquid at the tip−sample junction (*e.g.*, water, potassium hydroxide).[13−18] One recent study of Si tips on a polymer surface performed wear tests to large scanning distances (up to 750 m) and observed smooth and continuous evolution of the tip that was attributed to an atom-by-atom wear process.[19] Beyond silicon, other materials (usually coated onto a Si tip), including diamond, diamond-like carbon (DLC),

*Address correspondence to kturner@engr.wisc.edu.

Received for review February 6, 2010 and accepted June 07, 2010.

Published online June 24, 2010.
10.1021/nn100246g

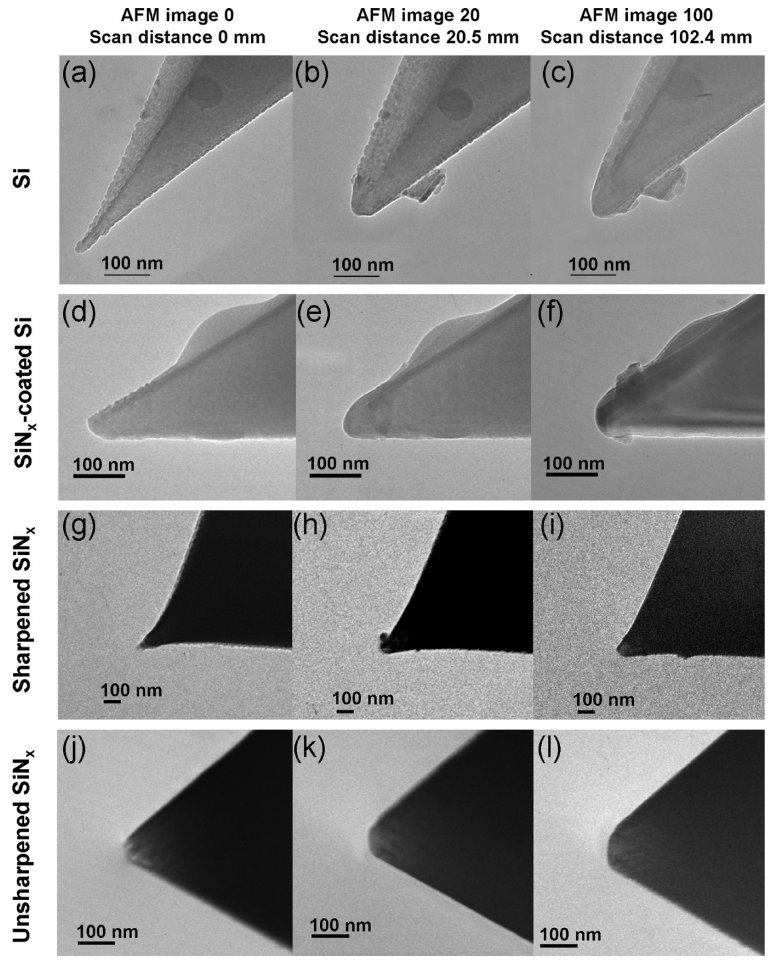

Figure 1. TEM images of the Si tip (a−c), the SiN_x-coated Si tip (d−f), the sharpened SiN_x tip (g−i), and the unsharpened SiN_x tip (j−l) before use, after acquiring 20 AFM images, and after acquiring 100 AFM images.

platinum, and polymers,[17,20−22] have been characterized in order to investigate nanoscale wear behavior of materials beyond those typically used for AFM probes. Most recently, tips made of ultrananocrystalline diamond (UNCD)[23,24] and DLC[8] have been fabricated and demonstrate a significant improvement in wear resistance over conventional Si-based probes. Advanced tip imaging techniques such as field emission scanning electron microscopy (FESEM) and high-resolution transmission electron microscopy (HRTEM) have been employed recently to characterize the structural changes of silicon and diamond-coated tips after repeated scanning.[18,25] The tip volume loss due to wear has been estimated through inverse imaging of the tip,[12] using blind reconstruction data,[21] direct imaging in AFM,[16] and from SEM and TEM images taken before and after wear scans.[9,18]

While these studies have illustrated the susceptibility of AFM tips to degradation *via* wear and demonstrated multiple approaches for characterizing tip geometry, there are several important limitations. First, in much of the previous work, both the tip and the surface experienced wear due to the modest hardness of the surfaces on which the tip was scanned. This adds complexity to accurately quantifying the wear of the tip through techniques such as blind reconstruction and inverse imaging. Systematic measurements of tip geometry and volume loss during the course of wear tests that are free of artifacts due to changes of the surface are essential for quantifying the nanoscale wear of tips. Second, the previous body of work has demonstrated many different techniques to characterize the tip geometry, but it has not provided a careful comparison between the different methods that allow the accuracy of the techniques to be verified. Finally, no study has systematically performed wear measurements under the action of adhesive forces alone (*e.g.*, zero externally applied force), the condition that is typically used in contact-mode AFM measurements. Adhesive forces between the tip and sample are significant, and substantial wear can occur under solely these forces.[26]

RESULTS AND DISCUSSION

Four types of commonly used, commercially available AFM tips were scanned on the sample in contact mode under adhesion forces alone for a total travel distance of 102.4 mm over the course of 100 images: (1) a single-crystalline silicon tip ("Si"), with a high aspect ra-

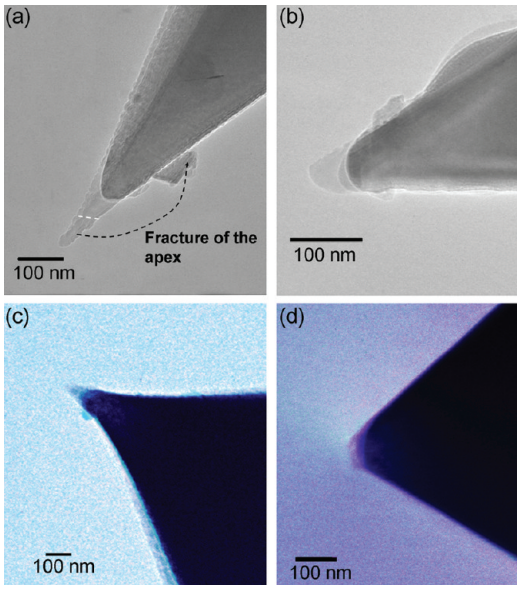

Figure 2. Overlaid TEM images of the Si tip (a), SiN_x-coated Si tip (b), sharpened SiN_x tip (c), and unsharpened SiN_x tip (d) before use, after acquiring 20 AFM images, and after acquiring 100 AFM images. The overlap of TEM images shows the evolution of tip geometry during scanning.

tio geometry resulting from a reactive ion etching (RIE) process; (2) a similar RIE-etched single-crystalline silicon tip with a silicon nitride coating ("SiN_x-coated Si"); (3) a sharpened silicon nitride tip with a pyramidal shape produced by depositing SiN_x into an oxidation-sharpened Si mold[27] ("sharpened SiN_x"); and (4) an unsharpened silicon nitride tip made by depositing SiN_x in a silicon mold ("unsharpened SiN_x"). At periodic intervals during the scanning, the tip geometry and tip−sample interaction were monitored using a combination of TEM, pull-off force measurements, and tip radius measurements obtained through a blind reconstruction.

The sample surface used for all measurements was a hard ultrananocrystalline diamond (UNCD) film deposited on a Si substrate. The UNCD sample serves three roles: as a hard material that wears the tip without becoming worn itself; as a sample with topographic features that allow the imaging performance of the tip to be assessed; and as a tip shape calibration sample whose small-scale roughness allows the tip geometry to be determined using the blind reconstruction method. The commercially available SPIP software package was used for performing the blind reconstruction (see Experimental Methods for details).

Tip Geometry and Imaging Performance. TEM micrographs of all four tips considered in this study are shown in Figure 1 at three different points in the wear test: before use, after 20 AFM images (sliding distance of 20.5 mm), and after 100 AFM images (sliding distance of 102.4 mm). The unworn Si tip started with a sharp apex with a radius of less than 10 nm, as shown in Figure 1a. This shape leads to the change in contrast along the shank of the tip seen in Figure 1a−c. After traveling a distance of 20.5 mm on the UNCD surface, the tip is significantly blunter. It is clear that the tip fractured, as the original end portion of the tip is attached to the side wall of the remaining tip in the image (Figure 1b). The fracture of Si tips in this manner was observed to occur frequently in subsequent tests. As the travel distance increased to 102.4 mm, little tip wear was observed (Figure 1b,c). However, additional debris and contamination became attached to the lower side of the tip (Figure 1c).

The SiN_x-coated Si tip, with a larger initial tip radius of ~15 nm due to the silicon nitride coating, showed gradual tip wear (Figure 1d−f). Contrast differences in the TEM micrographs indicate the existence of the SiN_x layer, and the large bump on the upper side provides a reference to track the evolution of the tip due to wear. The sharpened and unsharpened monolithic SiN_x tips both showed continuous gradual wear and the accumulation and loss of contaminant particles attaching on the side of the tip over the course of the wear test (Figure 1g−l).

The TEM images at different scan intervals for each tip are aligned and overlaid in Figure 2 to allow for better visualization of the changes in tip geometry over the course of the wear tests. As shown in Figure 2a, the Si tip experienced a significant change in geometry and loss of material during the first 20.5 mm of sliding, largely due to tip fracture, and then exhibited relatively little material loss from 20.5 to 102.4 mm. In contrast, the other three tips appear to exhibit gradual and progressive wear over the 102.4 mm scan distance.

The corresponding 3-D AFM topography images of the UNCD surfaces acquired with the four tips at different points in the wear test are shown in Figure 3. Despite the small initial tip radius (less than 10 nm) of the Si tip observed by TEM prior to AFM imaging (Figure 1a), the first AFM image obtained in Figure 3a does not exhibit better resolution than the first topographic images acquired with the other tips that have radii at least twice as large (Figure 3d,g,j). Also, Figure 3a,b contains repeated, slanted features, indicative of tip artifacts corresponding to the cleavage plane of the fractured Si tip denoted by the white dashed line in Figure 2a, suggesting that the tip fractured during the tip engaging process. The measurements with the three SiN_x probes show a gradual decrease in AFM image resolution with increasing scan distance (Figure 3d−l); however, the degradation of resolution for the unsharpened pyramidal SiN_x probe shown in Figure 3l is noticeably larger than for all of the sharpened tips (Figure 3c,f,i).

Quantification of Tip Radius and Adhesive Forces. Figure 4a shows the tip radius determined from both TEM observation and blind reconstruction for all four tips as a function of sliding distance, as detailed in the Experimental Methods section. In general, there is good agreement between the radii extracted from the two

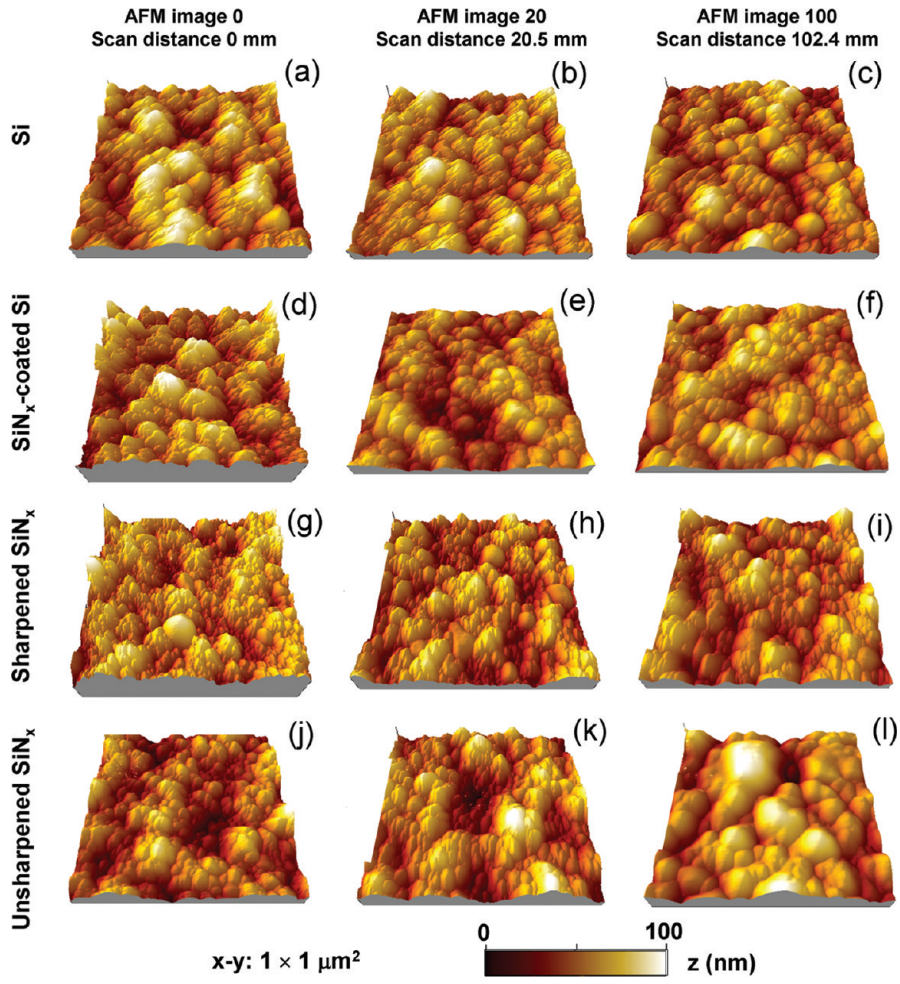

Figure 3. AFM topography images of 1 × 1 μm² UNCD surfaces acquired by the Si tip (a−c), the SiN_x-coated Si tip (d−f), the sharpened SiN_x tip (g−i), and the unsharpened SiN_x tip (j−l) before wear, after acquiring 20 AFM images, and after acquiring 100 AFM images. The height range (*z*-range) for all images is 100 nm.

methods (within 20%). This is the first report comparing direct TEM imaging of an AFM tip at the <10 nm scale with tip geometries obtained using blind reconstruction. A clear trend of increasing tip radius with sliding distance is observed for all probes, with a nearly 3-fold increase in radius observed over the course of the wear test for some tips. In addition, the rate of increase of tip radius with scanning distance slows progressively over the course of the test.

Adhesive forces between the tip and sample were determined by pull-off force measurements (also commonly referred to as force−distance curves) periodically throughout the wear scans. The pull-off force as a function of sliding distance is plotted in Figure 4b. The pull-off forces increase by more than a factor of 2 for all of the monolithic SIN_x tips during the course of the wear test. The pull-off force of the SiN_x-coated Si tip increases by a factor of 2.8 from images 40 to 60 and then decreases dramatically between images 60 and 70. Using a contact mechanics analysis, as explained in the Experimental Methods section, the work of adhesion values (Figure 4c) between the tips and sample surface were calculated based on the tip radii from blind reconstruction (Figure 4a) and the pull-off forces (Figure 4b). The overall work of adhesion values remained largely constant during the 100 image wear tests, with the exception of the Si tip at the beginning of test, and the SiN_x-coated Si tip between images 40 and 60. For the tip materials and TEM imaging conditions used here, no observable changes to the tip occur due to exposure of the tip to the TEM.

Fracture and Coating Failure. The comparable initial resolution between the high aspect ratio Si tip and the other larger radius tips as well as the slanted artifacts that appear in the first AFM images (Figure 3a) suggest that the fracture of the Si tip apex likely occurred during the initial contact between the tip and the UNCD surface. This observation may also explain the high work of adhesion of the Si tip at the beginning of the wear test shown in Figure 4c. Specifically, the newly exposed silicon surface will rapidly oxidize and hydrolyze, leading to a polar and hydrophilic surface with large surface energy. With time, molecular contamination will alter the surface of the tip and reduce the surface energy. This effect is well-documented for freshly cleaned silicon wafers.[28]

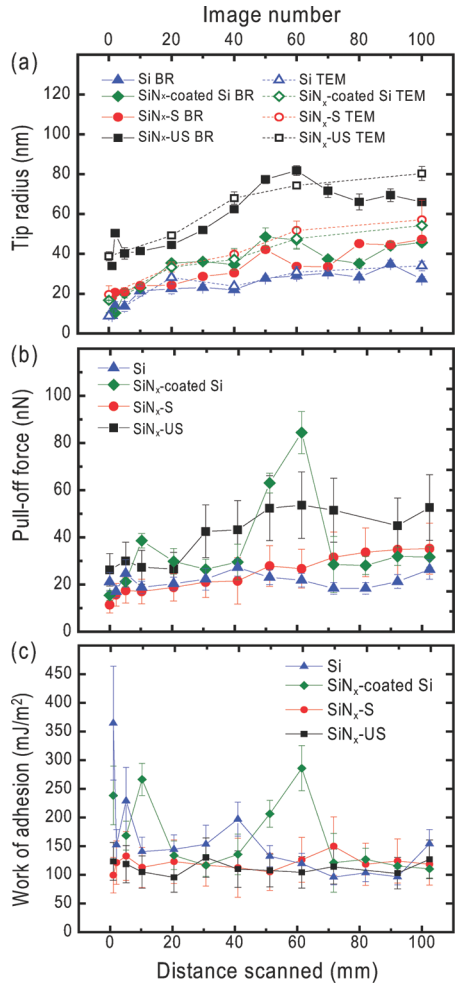

Figure 4. Plots of tip radius (a), pull-off force (b), and work of adhesion (c), as a function of distance scanned for the four tips.

The TEM and blind reconstruction images of the tip indicate that the SiN_x-coated Si tip experiences a gradual change in tip shape with scanning. However, the changes in the work of adhesion of the SiN_x-coated Si tip are more complex and suggest a change in both geometry and surface chemistry with scanning. The dramatic increase in work of adhesion for the SiN_x-coated Si tip starting at scan 50 can be better understood by examining the TEM images of the tip near the transition. In Figure 5, the work of adhesion data for the SiN_x-coated Si tip is replotted along with the corresponding high-magnification TEM images of the tip apex at scans 0, 60, and 100. At scan 60, the SiN_x coating appears to be intact on the sides of the tip but is completely removed at the bottom, leaving the underlying Si exposed. As with the freshly fractured Si tip, this Si surface, when newly exposed, would be expected to have a higher surface energy and would thus lead to a higher work of adhesion between the tip and surface, as was observed. After further time and scanning, the exposed Si surface will experience further wear and may become passivated. This results in a reduction of the work of adhesion. A layer covering the Si at the bottom of the tip can be clearly seen in the TEM image taken after image 100 (Figure 5).

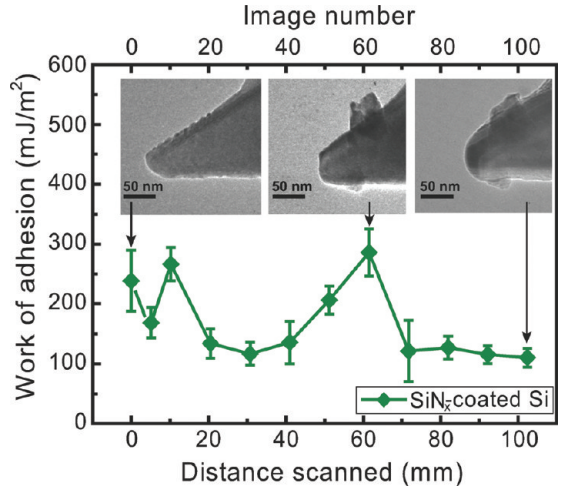

Figure 5. Work of adhesion as a function of sliding distance for the SiN_x-coated Si tip. The insets are TEM images corresponding to the tip before scanning, when the coating is unworn and low adhesion is observed; after 60 scans, when the coating has failed and adhesion is high; and after 100 scans, when the surface becomes passivated and adhesion decreases.

Assessment of Tip Geometry Characterization Methods. TEM and blind reconstruction from AFM topography images are used to characterize the tip geometry over the course of the wear test. There are several factors that must be considered when comparing the tip radius measurements from the two methods because of the positioning of the cantilever in the AFM (Figure 6a) and the mounting of the probe in TEM. First, as shown in Figure 6a, the raster scan direction (*x*-direction) in all AFM images (Figure 3) is perpendicular to the long axis of the cantilever. However, the *y*-direction (the slow scan direction in the AFM) is the direction of TEM profiles, a constraint imposed by mounting the cantilever in the TEM. Therefore, tip profiles reconstructed from the AFM image in the *y*-direction are the only profiles that may be meaningfully compared to the TEM images. As a result, reconstruction in the slow scan direction (*y*-direction), which is more prone to noise, is critical. To achieve accurate reconstructions, line-wise leveling and Fourier filtering to reduce the noise in the slow scan direction are used prior to blind reconstruction. If high-frequency noise is incorporated in the blind reconstruction, significant underestimation of the tip radius can occur. With this process, 3-D reconstructions of the tip, as shown in Figure 6b, are obtained. For most tips in the current study, the 3-D reconstructions appear nearly axisymmetric and the symmetry does not change significantly over the course of the wear test. Thus, only the reconstructed profiles and radii in the *y*-direction are extracted from the 3-D data and reported.

The other important factor in comparing TEM-measured tip profiles with blind reconstruction is that the AFM cantilever is held at a non-negligible angle

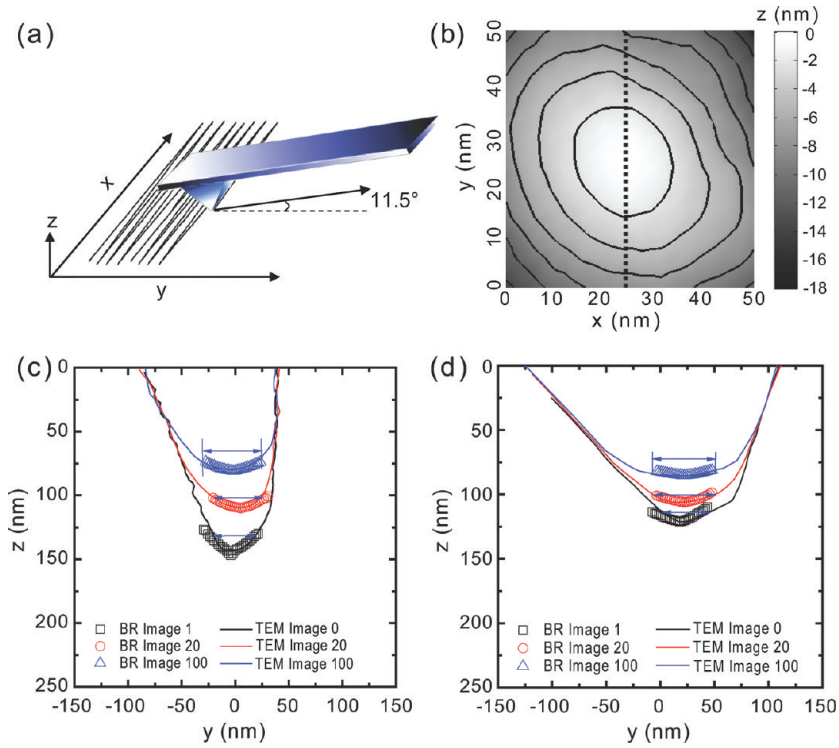

Figure 6. (a) Schematic of an AFM cantilever during AFM scanning showing incline of cantilever with respect to the sample. (b) Example of 3-D tip reconstruction for the SiN_x-coated tip at scan 100. The dashed line indicates the line along which the profile is extracted for comparison to TEM. (c,d) Comparison of the tip profiles measured by TEM and blind reconstruction ("BR") for (c) the SiN_x-coated Si probe and (d) the unsharpened SiN_x before use, after acquiring 20 images, and after acquiring 100 images.

with respect to the plane of the sample surface (nominally 11.5° in the Veeco Multimode AFM used to obtain the images in this study), as shown in Figure 6a. Along with the bending of the cantilever from residual strain effects (usually less than 0.5°), the tilt angle of the cantilever influences the contact point between the apex of the AFM tip and the sample and determines the overall orientation of the tip with respect to the surface. As such, when comparing the TEM profiles to the blind reconstruction, the TEM profiles are rotated by 11.5° with respect to the central axis of the tip. This is done for the TEM profiles shown in Figure 6, and this rotation is essential for obtaining good agreement between the TEM and blind reconstruction.

The TEM and blind reconstruction profiles are compared in Figure 6c,d for two of the tips characterized. The TEM profiles from different points in the wear test were adjusted vertically such that the unworn region of the shanks of the tips overlapped. The tip profiles from blind reconstruction agree very well with the TEM results for appropriate ranges (denoted by arrows).

These two methods of tip geometry characterization have their respective advantages and disadvantages. TEM is time consuming and requires that the wear scans be stopped and the cantilever be removed from the AFM, in contrast to blind reconstruction, which can be performed directly from AFM topography images. However, blind reconstruction requires careful selection of input parameters as discussed in detail in the Experimental Methods section. Perhaps the most important distinction between blind reconstruction and TEM is the portion of the tip that is measured. As seen in Figure 6c,d, blind reconstruction using the UNCD sample only allows a small portion of the tip geometry near the apex to be determined. This limitation is imposed by the relatively small scale of the roughness features on the UNCD sample. As such, blind reconstruction from images of a sample with fine scale roughness can be used to determine the detailed tip geometry at the apex, which determines imaging performance, but cannot be used to measure larger geometric and volume changes that are critical to determine wear rates. However, the larger scale TEM images provide a fiduciary reference (the unworn sides of the tip far from the apex, or the cantilever itself) from which the volume change can be determined.

Volume Loss and Wear Mechanisms. As discussed above, the TEM profiles of the tip can be used to estimate the volume loss over the course of a wear test. Figure 7 demonstrates the progressive wear of tips by comparing TEM profiles taken after scanning 20, 40, 60, and 100 AFM images scanned. The volume loss is estimated by subtracting the volume of the tip at each scan from that of the original unworn tip. The tip volume is calculated by assuming the tip comprises circular disk-shaped elements with a diameter equal to the measured tip width in the *y*-direction and then summing the volumes of all elements. The resulting volume loss as a function of

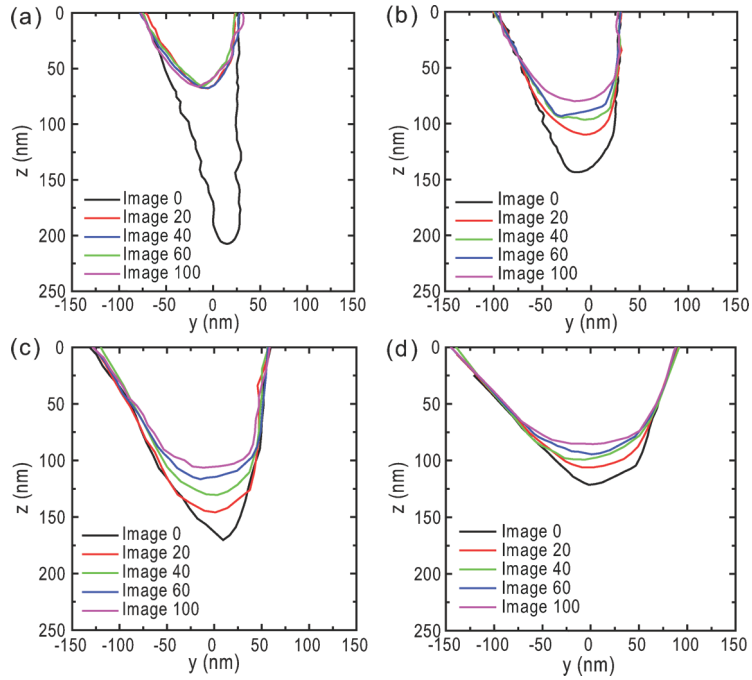

Figure 7. Profiles obtained by TEM of sharpened Si (a), SiN_x-coated Si (b), sharpened SiN_x (c), and unsharpened SiN_x (d) tips before wear, and after acquiring 20, 40, 60, and 100 AFM images.

distance scanned is shown in Figure 8a along with a visualization of one of the bodies used for volume calculation. The uncertainty in overlap of the TEM images and the resolution of the TEM images are used to determine the uncertainty in the volume loss calculations, denoted by the error bars in Figure 8a.

Archard's wear law is a first-order phenomenological model that uses a single parameter, the wear rate k, to describe the volume loss, ΔV, due to sliding under constant normal load F over sliding distance d:

$$\Delta V = kFd \quad (1)$$

In the tip−sample contacts in the current tests, the load on the tip is due to the adhesive force acting on the tip. As the adhesive forces vary with the size of the tip, the wear rate was calculated for each test interval (*i.e.*, 0−20.5, 20.5−41 mm, *etc.*) over which ΔV could be determined from the TEM measurements. The wear rate was calculated based on ΔV measured from TEM, the applied force determined from the average adhesive force over the test interval, and the scan distance based on distance specified for the scans. The calculated wear rates are shown in Figure 8b; the error bars represent the uncertainty based on a propagation of error calculation that combines uncertainty in the volume loss, force, and scan distance values. The wear rate for the single-crystalline Si tip over the first interval is marked differently in Figure 8b as the volume of material lost during the first 20 scans is due to a combination of both fracture and gradual wear. The wear rate

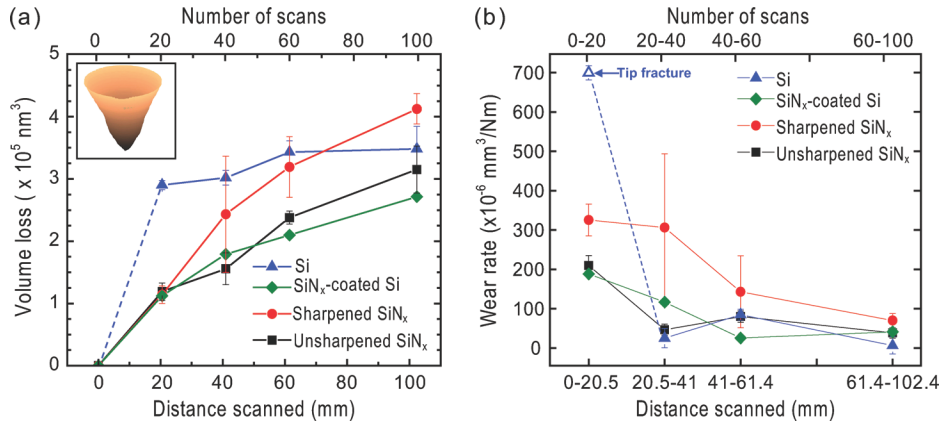

Figure 8. (a) Volume loss as a function of the sliding distance for all four tips. The inset shows a 3-D illustration of the body used for volume calculation of the sharpened SiN_x tip before wear scan. The dotted line for the first interval of the Si tip indicates that the volume loss is due to both fracture and wear. (b) Archard's wear rate calculated at scan intervals over which volume loss is measured by TEM. The point shown with an open symbol is a wear rate that includes volume loss due to both fracture and progressive wear.

for the Si tip is high in the first interval and calculated for reference but cannot be meaningfully compared to other wear rates reported in Figure 8b because of the significant fraction of the volume loss that occurred due to fracture.

For the monolithic SiN_x tips, the SiN_x-coated tip, and the Si tip after the 20.5 mm scan distance, the TEM and blind reconstruction data suggest a gradual change in tip shape and loss of material with increasing scan distance. This is consistent with mechanisms involving the progressive removal of atoms individually or in small clusters through local bond breaking.[19] The wear rates vary from 10^{-6} to 10^{-4} mm^3/Nm over the course of the wear tests and, in general, decrease with increasing scanning distance. Gotsmann and Lantz[19] have noted that as the tip becomes blunter, the contact stresses become less and the wear rate should decrease. This occurs even though the total load increases with scan distance due to the higher adhesive load that results from a larger tip. This is because the adhesive force is increasing linearly with the tip radius, R, while the contact area increases superlinearly with tip radius (for a Derjaguin−Müller−Toporov contact model, the contact area at zero load is proportional to $R^{4/3}$, thus the mean contact pressure is proportional to $R^{-1/3}$). The reduction of wear rate with increasing tip size observed clearly indicates the role that stress plays in controlling nanoscale wear.

In addition to stress, we note that the wear rates of the silicon-based probes may be affected by the presence of water. The wear tests reported here were completed in a normal laboratory environment in which relative humidity varied from 20 to 50% and was not controlled. Water molecules tend to absorb and decompose on the SiO_x layer on Si and SiN_x tips and can increase wear by enhancing bond breaking of Si atoms.[29,30]

CONCLUSIONS

To systematically examine the nanoscale wear behavior of AFM tips, a protocol that consists of a series of contact-mode AFM scans over hard UNCD surfaces in combination with multiple tip characterization approaches was developed and demonstrated. Quantitative agreement between tip dimensions obtained from blind reconstruction and TEM imaging was established. Changes in the behavior of different AFM tips were monitored over the course of wear tests using TEM, adhesive pull-off force measurements, and tip radius estimation through blind reconstruction. This wear characterization protocol was applied to four types of commercial Si and SiN_x AFM tips. Multiple mechanisms for tip degradation were observed, including tip fracture, coating failure, and gradual wear. The results demonstrate that adhesive forces alone are strong enough to modify and, in some cases, destroy Si and SiN_x tips after a small number of AFM scans. In addition to reducing image resolution, the tip fracture and coating failure result in a transient increase in the work of adhesion and, correspondingly, the contact forces between a tip and sample. This will affect the performance of the tip in many applications, including imaging and nanomanufacturing.

The combination of approaches used for tip characterization throughout the wear tests in this work provides a powerful and reliable methodology for obtaining a quantitative understanding of the nanoscale degradation of AFM tips with scanning. Blind reconstruction, while providing tip geometry data over a limited portion of the tip, is convenient and allows the 3-D tip geometry to be determined from each wear scan without additional measurements. The combination of the pull-off force measurements and tip radius estimated from blind reconstruction permits the work of adhesion to be calculated, which is helpful for identifying changes in surface condition due to events such as tip fracture and coating failure. Finally, direct TEM imaging of the tip, which is the only measurement that cannot be done in the AFM, provides a detailed picture of the geometry and structure of the tips. The TEM allows large-scale changes in tip geometry to be observed and, as a result, permits the volume loss of a tip to be quantified. The information provided by the combination of the techniques permits a thorough measurement of nanoscale tip degradation and provides opportunities to explore the fundamentals of nanoscale wear mechanics.

EXPERIMENTAL METHODS

Before scanning, the planar dimensions and curvature due to residual stress of the AFM cantilevers were measured using optical microscopy and white light interferometry (Zygo NewView 5000), respectively. Cantilever thickness, tip morphology, and tip radius along the long axis (*y*-direction of AFM scans) of the cantilever were evaluated by TEM (JEOL 200CX). The spring constants K of the AFM cantilevers used in each experiment were calculated based on the measured dimensions of the probes.[31]

A Digital Instruments MultiMode AFM was used to perform the wear scans. In each wear test, 100 contact-mode images (1 × 1 μm^2 area) on a UNCD surface were acquired by raster scans, consisting of 512 lines. The fast scan direction (*x*-direction) was perpendicular to the long axis of the cantilever. During a single 1 × 1 μm^2 scan, the tip is scanned 512 μm in the positive *x*-direction and 512 μm in the negative *x*-direction. The UNCD sample ("Aqua 25", Advanced Diamond Technologies, Romeoville, IL) was measured to have an rms roughness of ~9 nm over a 1 *x* 1μm^2 area. The random features of its surface are suitable for tip characterization *via* blind reconstruction. Because of its high mechanical strength,[32,33] it wears a negligible amount compared to the tips. All tests were performed under zero applied load (*i.e.*, zero cantilever deflection), resulting in loading that is solely due to adhesive forces between the tip and sample. Calibration of the zero load position was repeatedly checked as described below. The scanning distance and speed of the tip

were 1.024 mm per image (1×1 μm^2 scan) and 3.97 μm/s, respectively. The tests were performed in laboratory air at a temperature of about 20 °C. The relative humidity (RH) was not controlled but was measured in the experiments. The RH during the SiN_x-coated Si and the unsharpened SiN_x tests was ~50%, and the RH during the sharpened Si and sharpened SiN_x tests was ~20%.

The full tip geometry was characterized using TEM for each tip after acquiring 20, 40, 60, and 100 AFM images. Force−distance measurements were obtained after every 10 images at five different positions on a tetrahedral amorphous carbon (ta-C) sample that was positioned next to the UNCD sample to enable fast switching between the UNCD and ta-C samples. Pull-off measurements were made on ta-C, which has a similar surface energy but a much lower rms roughness (less than 1 nm) than UNCD, to reduce variation in the pull-off measurements that arise from topography variations. Because of thermal drift of the AFM signal and cantilever, the out-of-contact deflection signal corresponding to zero force between the tip and sample was measured and the feedback set point was adjusted to this value during the force−distance measurements. This ensured that the subsequent scans were always obtained in contact at zero net applied load. The pull-off deflection, δ, of the cantilever was determined from each of these force−distance measurements. The adhesive force F between the tip and sample was calculated using $F = K\delta$, where K is the cantilever's flexural spring constant.

The Derjaguin−Müller−Toporov (DMT) theory of contact mechanics[34] was used to calculate the work of adhesion between the tip and sample. According to the DMT model, the adhesive force between the tip and sample is

$$F = 2\pi WR \quad (2)$$

where W is the work of adhesion and R is the tip radius. The pull-off force measurements provide information about changes in both the work of adhesion and the tip radius while scanning. After the pull-off force measurements, the wear scan was resumed on a new area of the UNCD surface. The DMT model assumes that the tip and sample are homogeneous, isotropic, linear elastic materials, and that strains are small. The tip is assumed to be paraboloidal, with a radius much larger than the tip−sample contact radius and the normal elastic deformation of the contact. It also assumes the adhesive forces are long-ranged compared to the deformations they cause, which implies relatively stiff materials with low adhesion and small tips. In the studies presented here, the Tabor parameters μ_T were calculated, and the corresponding Maugis parameters $\lambda = 1.157$ μ_T for all four types of tip range from 0.066 to 0.13, indicating that the DMT model provides a reasonable estimate of the work of adhesion.[35,36]

The tip radius at each scan was estimated from the measured topography images of the UNCD surface using the blind reconstruction method,[37] a process based on convolution/deconvolution theory, using the commercially available Scanning Probe Image Processor (SPIP v2.3, Image Metrology, Aps, Denmark) software. The tip profiles obtained from blind reconstruction were compared with TEM measurements (Figure 6) and the data ranges over which the two methods agrees well (<1 nm deviation) were fitted to a parabola using a least-mean-squares algorithm. The radius of curvature values were obtained from the parabolic fit using both the blind reconstruction measurements and TEM. Different ranges of tip profile within the range of deviation were compared, and the variation of fitted radius values was used as the error in the analysis.

Prior to reconstruction, the AFM images were processed using a first-order least-mean-square line-by-line correction flattening algorithm and a low-pass Fourier filter to eliminate artifacts from low-frequency drift and high-frequency noise, respectively. For the Fourier filter, a cutoff frequency of 1/(3.9 nm), which is the Nyquist cutoff frequency based on the spatial resolution of the image, was selected since higher spatial frequencies should not be present.

To reconstruct the tip geometry from the AFM images, SPIP requires four input parameters: reconstruction size, ignored lower value, number of iterations, and acceptance counts. The input parameters were systematically studied and were chosen as follows: (1) a tip reconstruction size of 27×27 pixels was chosen to reconstruct a reasonably large portion of the tip (54 nm wide); (2) the lower third of the z-height values, which are not likely to contribute useful information to the blind reconstruction, was ignored to eliminate unwanted influence from any sharp noise peaks recorded at those heights; (3) three iterations of the SPIP algorithm ensured full convergence of the results; and (4) the "acceptance level" for detection counts[38] was chosen on an image-by-image basis by selecting the most abrupt turning point in tip height confidence graphs[39] (chosen values ranged from 5 to 10).

Acknowledgment. This work was supported by NSF under STTR Grant Nos. 0638030 and 0823002, and NSF Awards CMMI-0826076 and CMMI-0825000. Additional facilities support was provided by NSF under DMR-0520527.

REFERENCES AND NOTES

1. Giesbers, A. J. M.; Zeitler, U.; Neubeck, S.; Freitag, F.; Novoselov, K. S.; Maan, J. C. Nanolithography and Manipulation of Graphene Using an Atomic Force Microscope. *Solid State Commun.* **2008**, *147*, 366–369.
2. Bullen, D.; Wang, X.; Zou, J.; Chung, S.-W.; Mirkin, C. A.; Liu, C. Design, Fabrication, and Characterization of Thermally Actuated Probe Arrays for Dip Pen Nanolithography. *J. Microelectromech. Syst.* **2004**, *13*, 594–602.
3. Senesi, A. J.; Rozkiewicz, D. I.; Reinhoudt, D. N.; Mirkin, C. A. Agarose-Assisted Dip-Pen Nanolithography of Oligonucleotides and Proteins. *ACS Nano* **2009**, *3*, 2394–2402.
4. Chimmalgi, A.; Grigoropoulos, C. P.; Komvopoulos, K. Surface Nanostructuring by Nano-/Femtosecond Laser-Assisted Scanning Force Microscopy. *J. Appl. Phys.* **2005**, *97*, 104319.
5. El Rifai, O. M.; Aumond, B. D.; Youcef-Toumi, K. Imaging at the Nano-scale. In Proceedings of the 2003 IEEE/ASME International Conference on Advanced Intelligent Mechatronics, Kobe, Japan, 2003; pp 715−722.
6. Yacoot, A.; Koenders, L. Aspects of Scanning Force Microscope Probes and Their Effects on Dimensional Measurement. *J. Phys. D: Appl. Phys.* **2008**, *41*, 103001.
7. Vettiger, P.; Cross, G.; Despont, M.; Drechsler, U.; Durig, U.; Gotsmann, B.; Haberle, W.; Lantz, M. A.; Rothuizen, H. E.; Stutz, R.; Binnig, G. K. The "Millipede"-Nanotechnology Entering Data Storage. *IEEE Trans. Nanotechnol.* **2002**, *1*, 39–54.
8. Bhaskaran, H.; Gotsmann, B.; Sebastian, A.; Drechsler, U.; Lantz, M. A.; Despont, M.; Jaroenapibal, P.; Carpick, R. W.; Chen, Y.; Sridharan, K. Ultralow Nanoscale Wear through Atom-by-Atom Attrition in Silicon-Containing Diamond-like Carbon. *Nat. Nanotechnol.* **2010**, *5*, 181–185.
9. Kim, K.-H.; Moldovan, N.; Ke, C.; Espinosa, H. D.; Xiao, X.; Carlisle, J. A.; Auciello, O. Novel Ultrananocrystalline Diamond Probes for High-Resolution Low-Wear Nanolithographic Techniques. *Small* **2005**, *1*, 866–874.
10. Wilson, N. R.; Macpherson, J. V. Carbon Nanotube Tips for Atomic Force Microscopy. *Nat. Nanotechnol.* **2009**, *4*, 483–491.
11. Khurshudov, A.; Kato, K. Wear of the Atomic Force Microscope Tip under Light Load, Studied by Atomic Force Microscopy. *Ultramicroscopy* **1995**, *60*, 11–16.
12. Bloo, M. L.; Haitjema, H.; Pril, W. O. Deformation and Wear of Pyramidal, Silicon-Nitride AFM Tips Scanning Micrometre-Size Features in Contact Mode. *Measurement* **1999**, *25*, 203–211.
13. Chung, K.-H.; Kim, D.-E. Fundamental Investigation of Micro Wear Rate Using an Atomic Force Microscope. *Tribol. Lett.* **2003**, *15*, 135–144.
14. Katsuki, F. Single Asperity Tribochemical Wear of Silicon by Atomic Force Microscopy. *J. Mater. Res.* **2009**, *24*, 173–178.
15. Katsuki, F.; Saguchi, A.; Takahashi, W.; Watanabe, J. The Atomic-Scale Removal Mechanism During Si Tip Scratching on Si and SiO_2 Surfaces in Aqueous KOH with

an Atomic Force Microscope. *Jpn. J. Appl. Phys.* **2002**, *41*, 4919–4923.
16. Maw, W.; Stevens, F.; Langford, S. C.; Dickinson, J. T. Single Asperity Tribochemical Wear of Silicon Nitride Studied by Atomic Force Microscopy. *J. Appl. Phys.* **2002**, *92*, 5103–5110.
17. Kwak, K. J.; Bhushan, B. Platinum-Coated Probes Sliding at up to 100 mm/s against Lead Zirconate Titanate Films for Atomic Force Microscopy Probe-Based Ferroelectric Recording Technology. *J. Vac. Sci. Technol., A* **2008**, *26*, 783–793.
18. Chung, K.-H.; Lee, Y.-H.; Kim, D.-E. Characteristics of Fracture During the Approach Process and Wear Mechanism of a Silicon AFM Tip. *Ultramicroscopy* **2005**, *102*, 161–171.
19. Gotsmann, B.; Lantz, M. A. Atomistic Wear in a Single Asperity Sliding Contact. *Phys. Rev. Lett.* **2008**, *101*, 125501.
20. Khurshudov, A. G.; Kato, K.; Koide, H. Nano-Wear of the Diamond AFM Probing Tip under Scratching of Silicon, Studied by AFM. *Tribol. Lett.* **1996**, *2*, 345–354.
21. Bhushan, B.; Kwak, K. J. Platinum-Coated Probes Sliding at up to 100 mm s^{-1} against Coated Silicon Wafers for AFM Probe-Based Recording Technology. *Nanotechnology* **2007**, *18*, 345504.
22. Agrawal, R.; Moldovan, N.; Espinosa, H. D. An Energy-Based Model To Predict Wear in Nanocrystalline Diamond Atomic Force Microscopy Tips. *J. Appl. Phys.* **2009**, *106*, 064311.
23. Liu, J.; Grierson, D. S.; Moldovan, N.; Notbohm, J.; Li, S.; Jaroenapibal, P.; O'Connor, S. D.; Sumant, A. V.; Neelakantan, N.; Carlisle, J. A.; Turner, K. T.; Carpick, R. W. Preventing Nanoscale Wear of Atomic Force Microscopy Tips through the Use of Monolithic Ultrananocrystalline Diamond Probes. *Small* **2010**, *6*, 1140–1149.
24. Fletcher, P. C.; Felts, J. R.; Dai, Z.; Jacobs, T. D.; Zeng, H.; Lee, W.; Sheehan, P. E.; Carlisle, J. A.; Carpick, R. W.; King, W. P. Wear-Resistant Diamond Nanoprobe Tips with Integrated Silicon Heater for Tip-Based Nanomanufacturing. *ACS Nano.* 2010, (Articles ASAP May 18, 2010- DOI:10.1021/nn100203d)
25. Chung, K.-H.; Kim, D.-E. Wear Characteristics of Diamond-Coated Atomic Force Microscope Probe. *Ultramicroscopy* **2007**, *108*, 1–10.
26. Kopycinska-Muller, M.; Geiss, R. H.; Hurley, D. C. Contact Mechanics and Tip Shape in AFM-Based Nanomechanical Measurements. *Ultramicroscopy* **2006**, *106*, 466–474.
27. Albrecht, T. R.; Akamine, S.; Carver, T. E.; Quate, C. F. Microfabrication of Cantilever Styli for the Atomic Force Microscope. *J. Vac. Sci. Technol., A* **1990**, *8*, 3386–3396.
28. Roche, A.; Wyon, C.; Marthon, S.; Ple, J. F.; Olivier, M.; Rochat, N.; Chabli, A.; Danel, A.; Juhel, M.; Tardif, F. Detection of Organic Contamination on Silicon Substrates: Comparison of Several Techniques. In *Characterization and Metrology for ULSI Technology 2000*; American Institute of Physics: Woodbury, NY, 2001; pp 297−301.
29. Bunker, B. C.; Haaland, D. M.; Michalske, T. A.; Smith, W. L. Kinetics of Dissocialtive Chemisrption on Strained Edge-Shared Surface Defects on Dehydroxylated Silica. *Surf. Sci.* **1989**, *222*, 95–118.
30. Zhu, T.; Li, J.; Lin, X.; Yip, S. Stress-Dependent Molecular Pathways of Silica-Water Reaction. *J. Mech. Phys. Solids* **2005**, *53*, 1597–1623.
31. Clifford, C. A.; Seah, M. P. The Determination of Atomic Force Microscope Cantilever Spring Constants *via* Dimensional Methods for Nanomechanical Analysis. *Nanotechnology* **2005**, *16*, 1666–1680.
32. Krauss, A. R.; Auciello, O.; Gruen, D. M.; Jayatissa, A.; Sumant, A.; Tucek, J.; Mancini, D. C.; Moldovan, N.; Erdemir, A.; Ersoy, D.; Gardos, M. N.; Busmann, H. G.; Meyer, E. M.; Ding, M. Q. Ultrananocrystalline Diamond Thin Films for MEMS and Moving Mechanical Assembly Devices. *Diamond Relat. Mater.* **2001**, *10*, 1952–1961.
33. Sumant, A. V.; Grierson, D. S.; Gerbi, J. E.; Birrell, J.; Lanke, U. D.; Auciello, O.; Carlisle, J. A.; Carpick, R. W. Toward the Ultimate Tribological Interface: Surface Chemistry and Nanotribology of Ultrananocrystalline Diamond. *Adv. Mater.* **2005**, *17*, 1039–1045.
34. Derjaguin, B. V.; Muller, V. M.; Toporov, Y. P. Effect of Contact Deformations on the Adhesion of Particles. *J. Colloid Interface Sci.* **1975**, *53*, 314–326.
35. Grierson, D. S.; Flater, E. E.; Carpick, R. W. Accounting for the JKR−DMT Transition in Adhesion and Friction Measurements with Atomic Force Microscopy. *J. Adhes. Sci. Technol.* **2005**, *19*, 291–311.
36. Maugis, D. Adhesion of Spheres: The JKR-DMT Transition Using a Dugdale Model. *J. Colloid Interface Sci.* **1992**, *150*, 243–269.
37. Villarrubia, J. S. Algorithms for Scanned Probe Microscope Image Simulation, Surface Reconstruction, and Tip Estimation. *J. Res. Natl. Inst. Stand. Technol.* **1997**, *102*, 425–454.
38. Detection counts: A threshold parameter to eliminate the effect of high-frequency noise. The "acceptance level" establishes the tolerance of the levels of inconsistency between the image and the reconstructed tips.
39. Tip height confidence graphs: Reconstructed tip heights as a function of detection counts.